JOURNAL OF GEOPHYSICAL RESEARCH, VOL. 114, A00E03, doi:10.1029/2008JA013720, 2009

Comparison of acceleration, expansion, and brightness of sprite streamers obtained from modeling and high-speed video observations

N. Y. Liu,[1] V. P. Pasko,[2] K. Adams,[2] H. C. Stenbaek-Nielsen,[3] and M. G. McHarg[4]

Received 2 September 2008; revised 10 December 2008; accepted 15 January 2009; published 26 March 2009.

[1] We compare sprite streamer modeling results with high-speed video recordings of sprites made with 50-μs temporal resolution. Both the modeling results and the sprite videos show that sprite streamers propagate with acceleration and expansion during the initial stage of sprite development. The acceleration computed from the modeling for the applied electric fields close to the conventional breakdown threshold field is on the order of $(0.5–1) \times 10^{10}$ m s^{-2} and is in good agreement with the peak values observed experimentally. We further discuss the effects of different spatial and temporal resolutions of an observational system on the visual appearances of sprite streamers. It is found that the large variation in brightness of sprites estimated from several observational studies can be directly attributed to different temporal and spatial resolutions of used instruments. Mainly due to the increasing radius of the streamer head of an accelerating streamer, the brightness of the streamer head increases as well. The comparison results demonstrate that the brightness of a sprite streamer head increases exponentially with time and can span more than 4 orders of magnitude in a very short period of about 1 ms. We propose a method for remote sensing of the sprite-driving electric field in the mesospheric and lower ionospheric region by measuring the rate of the change of the brightness.

Citation: Liu, N. Y., V. P. Pasko, K. Adams, H. C. Stenbaek-Nielsen, and M. G. McHarg (2009), Comparison of acceleration, expansion, and brightness of sprite streamers obtained from modeling and high-speed video observations, *J. Geophys. Res.*, *114*, A00E03, doi:10.1029/2008JA013720.

1. Introduction

[2] Sprites are large air discharges appearing above thunderclouds typically following intense positive cloud-to-ground (CG) lightning discharges [*Sentman et al.*, 1995]. They are initiated when the lightning induced quasi-static electric field exceeds the local breakdown threshold field in the mesospheric/lower ionospheric region in the Earth's atmosphere [*Pasko*, 2007]. In high spatial resolution images the streamer type of air discharges is identified as a basic component of sprites [e.g., *Gerken et al.*, 2000; *Gerken and Inan*, 2002, 2003].

[3] Streamer discharges are known at atmospheric pressure as the precursor of spark discharges. They are found in many plasma discharge systems in natural phenomena and in practical applications [*Ebert et al.*, 2006]. The theory of streamer discharge was introduced back in the early last century [e.g., *Loeb and Meek*, 1940]. However, because of their transient nature, resolving the detailed structure of streamers greatly relied on theoretical and numerical work until recent applications of fast observational instruments in streamer experiments. High temporal resolution ($\sim$1 ns) images have been recently obtained for streamer development in laboratory experiments at atmospheric pressure, which reveal bright, localized streamer heads markedly different from continuous luminous channels obtained because of time integration effects on longer timescales [*van Veldhuizen and Rutgers*, 2002; *van Veldhuizen et al.*, 2002; *Briels et al.*, 2006; *Ebert et al.*, 2006].

[4] Instrumental systems utilized in early sprite observations normally had the same temporal resolution as standard TV ($\sim$30 ms) [e.g., *Sentman et al.*, 1995]. High-speed video observations of sprites taken at frame rates >1000 fps provided detailed information on the temporal development of sprites and the characteristics of sprite streamers [*Stanley et al.*, 1999; *Moudry et al.*, 2002, 2003; *McHarg et al.*, 2002, 2007; *Marshall and Inan*, 2005; *Cummer et al.*, 2006; *Stenbaek-Nielsen et al.*, 2007]. One of the important conclusions derived from these high-speed video observations is that the speed of sprite streamers can reach a fraction of the speed of light. The observational work reported by *McHarg et al.* [2007] and *Stenbaek-Nielsen et al.* [2007] further demonstrates that sprite streamers accelerate and

[1]Geospace Physics Laboratory, Florida Institute of Technology, Melbourne, Florida, USA.
[2]Communications and Space Sciences Laboratory, Pennsylvania State University, University Park, Pennsylvania, USA.
[3]Geophysical Institute, University of Alaska, Fairbanks, Alaska, USA.
[4]Department of Physics, United States Air Force Academy, Colorado, USA.

0148-0227/09/2008JA013720$09.00

expand during their propagation. The exposure time for the sprite images obtained by *McHarg et al.* [2007] and *Stenbaek-Nielsen et al.* [2007] is 50 μs. The 50 μs for plasma discharges at the initiation altitude (typically 75–80 km) of sprites is equivalent to 1 ns at atmospheric pressure according to similarity laws [*Pasko et al.*, 1998; *Liu and Pasko*, 2004, 2006]. An excellent review of the evolution of the temporal resolution of the sprite observational systems is given in the work of *Sentman et al.* [2008].

[5] Although it has been suggested that sprites may be initiated through simultaneous up and down propagating streamers [*Liu and Pasko*, 2004], the recent observational evidence indicates that the preferential form of sprite initiation is through downward development of positive streamers launched in the region of the lower ledge of the Earth's ionosphere (see discussion of *Stenbaek-Nielsen et al.* [2007, and references therein]). The exact mechanism of initiation of sprite streamers remains unknown and may be related to formation of upwardly concave ionization regions near the lower ionospheric boundary associated with sprite halos [*Barrington-Leigh et al.*, 2001]. The initial appearance of positive streamers is likely realized because of a relatively slow application of the electric field at sprite altitudes ($\sim$1 ms) [*Marshall and Inan*, 2006; *Hu et al.*, 2007] coupled with lower propagation threshold for positive streamers in comparison with negative ones [*Pasko et al.*, 2000], which creates asymmetric conditions with predominant initial propagation of positive streamers. The different thresholds of propagation of positive and negative streamers in sprites have recently been supported by observations reported by *Taylor et al.* [2008]. These authors reported a measurement of a sprite event caused by a negative CG lightning discharge. This polarity of sprites is rarely observed and another notable report about negative sprites was made by *Barrington-Leigh et al.* [1999]. *Taylor et al.* [2008] compared sprites produced by positive and negative cloud-to-ground (CG) lightning discharges with approximately the same charge moment change magnitudes during the same storm and demonstrated that the positive CG produced sprites propagated to lower altitude.

[6] The purpose of this paper is to conduct a comparison of sprite streamer modeling with the high-speed video observations reported recently by *McHarg et al.* [2007] and *Stenbaek-Nielsen et al.* [2007]. We investigate the effects of different spatial and temporal resolutions of an observational system on the visual appearances of the captured sprite streamers. As has been noted in previous modeling work on streamers at atmospheric pressure [e.g., *Babaeva and Naidis*, 1997; *Kulikovsky*, 1997] and sprite streamers [*Liu and Pasko*, 2004], both the radius and the speed of a model streamer increase as it propagates in an electric field greater than the propagation threshold fields of streamers. We compare the acceleration of sprite streamers calculated from the modeling with that obtained from the high-speed video observations. The analysis of the high-speed sprite video observations indicates that the brightness of a sprite streamer head increases during the development of the streamer [*Stenbaek-Nielsen et al.*, 2007]. In this work we also compare the time evolution of brightness for observed and modeled streamers. This comparison leads to formulation of a method for remote sensing of the lightning induced electric field in the mesospheric and lower ionospheric regions of the atmosphere, which drives the sprite phenomenon.

2. Problem Formulation

[7] Several emission band systems of N_2 and N_2^+ are observed as being emitted from sprites. As discussed in many papers on sprite spectroscopy [e.g., *Sentman et al.*, 1995; *Mende et al.*, 1995; *Hampton et al.*, 1996; *Kanmae et al.*, 2007; *Pasko*, 2007; *Sentman et al.*, 2008], the emissions of sprite streamers are dominated by red emissions of the first positive band system of N_2 ($1PN_2$). However, for streamers at atmospheric pressure, blue emissions of the second positive band system of N_2 ($2PN_2$) are commonly observed in laboratory experiments [e.g., *Shcherbakov and Sigmond*, 2007], and are stronger than $1PN_2$ emissions according to modeling results [e.g., *Liu et al.*, 2008]. This difference is attributed to differences in quenching altitudes of $B^3\Pi_g$ (53 km) and $C^3\Pi_u$ (30 km) excited states of N_2, responsible for $1PN_2$ and $2PN_2$ emissions, respectively [*Liu et al.*, 2008]. In the present paper, we compare the modeling results on the intensity of $1PN_2$ emissions from sprite streamers with the high-speed sprite video observations, which are conducted by a camera having a passband of 400–900 nm with the maximum sensitivity at about 800 nm [*McHarg et al.*, 2007; *Stenbaek-Nielsen et al.*, 2007]. We consider the sprite images recorded by the camera as being predominantly due to $1PN_2$ emissions, consistent with the recent analysis by *Kanmae et al.* [2007].

[8] The streamer model employed in the present study is axisymmetric. The model equations consist of continuity equations of charged particles and Poisson's equation [*Liu and Pasko*, 2004, 2006]. The simulation domain is similar to that used by *Liu and Pasko* [2006]. However, the conducting sphere is placed next to the top boundary of the simulation domain, and the direction of the applied field is reversed. Thus a model positive streamer propagates in the negative z direction to be consistent with the downward propagating positive streamers normally observed in sprites. The top boundary of the simulation domain is at 75 km altitude, and the model streamer is initiated by placing a neutral plasma cloud with a spherically symmetric Gaussian spatial distribution centered at the axis of symmetry and 6 m below the top boundary. The distribution has a characteristic scale of 3 m and a peak density of 1.2×10^9 1/m^3. The simulation domain is discretized into a uniform grid with 1401×201 grid points in the z and r directions, respectively.

[9] To calculate the intensity of $1PN_2$ emissions, we compute the density of the $B^3\Pi_g$ excited state of N_2 leading to $1PN_2$ emissions at every time step and then obtain the volume emission rate by multiplying the density by the Einstein coefficient, which is the inverse lifetime of the $B^3\Pi_g$ excited state (quenching of the $B^3\Pi_g$ state at 75 km altitude is negligible). We finally convert the volume emission rate into Rayleighs (1 Rayleigh = 10^6 photons/cm^2 – column/s) by integrating the volume emission rate along a line of sight perpendicular to the streamer [e.g., *Liu and Pasko*, 2004].

3. Results and Discussion

3.1. Acceleration and Expansion of Streamers

[10] A positive streamer developing in an electric field of 30 N/N_0 kV/cm at 75 km altitude at $t = 300$ μs is shown in

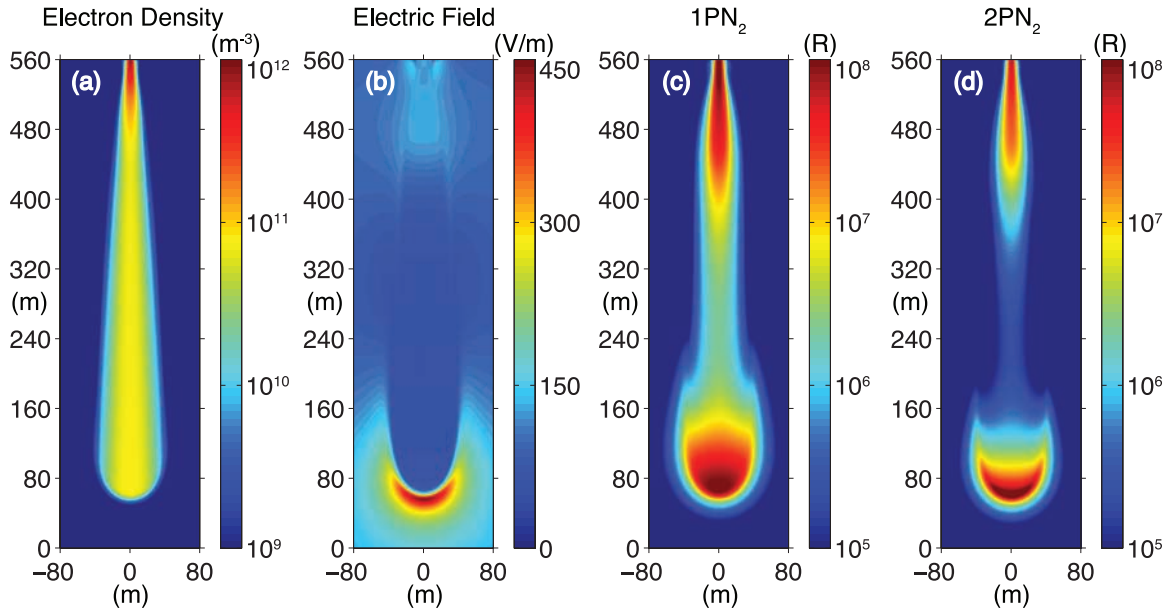

Figure 1. A cross-sectional view of (a) electron density, (b) electric field, (c) $1PN_2$ intensity, and (d) $2PN_2$ intensity for a downward-propagating positive streamer in an electric field of 30 N/N_0 kV/cm at 75-km altitude at t = 300 μs.

Figure 1. Here, N is air density at 75 km altitude and N_0 is air density at ground level. We note that in this model case the chosen value of the applied electric field is close to the conventional breakdown threshold of air defined by equality of ionization and dissociative attachment coefficients in air [e.g., *Raizer*, 1991, p. 135]. The expansion of the streamer is clearly indicated by the distribution of the electron density (Figure 1a). The maximum electric field in the streamer head is about 440 V/m or 4 times the conventional breakdown threshold field. According to Figures 1c and 1d, the maximum intensities of $1PN_2$ and $2PN_2$ are very similar, however the source size of $1PN_2$ is larger than that of $2PN_2$. The emissions are highly enhanced in the streamer head in comparison with the streamer channel.

[11] Figure 2 shows a sequence of intensity distributions of $1PN_2$ for the model positive streamer shown in Figure 1. The time interval between two successive images is 20 μs. Each image represents the emission intensity in Rayleighs at the specific moment of time shown at the top of the image. The formatting of this Figure 2 is consistent with streamer progression obtained experimentally in high-speed videos and shown in Figure 2 of *Stenbaek-Nielsen et al.* [2007]. The trajectory of the streamer head follows a parabolic curve indicating the accelerating motion of the streamer, consistent with similar effect observed by *Stenbaek-Nielsen et al.* [2007, Figure 2]. The size of the streamer head keeps increasing and the radius of the visible head reaches about 50 m at t = 300 μs. In the model, the positive streamer with downward propagating direction is initiated because of the introduction of the neutral plasma cloud in the high field region below the top boundary of the simulation domain. On the other hand, the observed streamer is initiated at the lower ionospheric boundary, so that no upward propagating negative streamers formed because the lightning induced electric field in this region relaxes on a timescale shorter than the streamer formation time [*Pasko et al.*, 1998].

[12] The speed and acceleration of a model streamer depend on the applied electric field [*Babaeva and Naidis*, 1997; *Liu and Pasko*, 2004]. Figure 3 illustrates the speed of the model streamer as a function of time for two different applied electric fields: 30 N/N_0 kV/cm and 25 N/N_0 kV/cm. The points represent the speeds computed from the modeling results at the corresponding moments of time. The streamer in the stronger field propagates faster than the one in the lower field case. The acceleration of the streamer is not constant and increases as time progresses. The average accelerations of the two model streamers are 10^{10} m/s^2 and 4.6 $\times$ 10^9 m/s^2, respectively, which correspond to the slopes of the solid lines in Figure 3. These two values agree well with the high-speed video observations by *McHarg et al.* [2007], who reported that the accelerations of sprite streamers are often on the order of 10^{10} although the values could vary from 10^5 to 10^{10} m/s^2.

[13] We can further illustrate the variation of the streamer speed as a function of time by considering Figure 4. According to Figure 4, the logarithm of the speed linearly depends on time. In agreement with the previous modeling results by *Babaeva and Naidis* [1997], the speed increases linearly with the streamer length with slopes 5.8 $\times$ 10^3 and 3.5 $\times$ 10^3 1/s for the fields 30 N/N_0 kV/cm and 25 N/N_0 kV/cm, respectively.

[14] We emphasize that model simulations presented in this paper are obtained in a relatively small simulation domain with vertical dimension ~550 m. However, the simple linear dependencies documented in Figure 4 can be directly extrapolated to larger distances and longer timescales if an assumption is made that the reduced electric field (E/N) remains the same. As demonstrated in section 3.3 the model streamers in the present work correspond to initial stage of development of

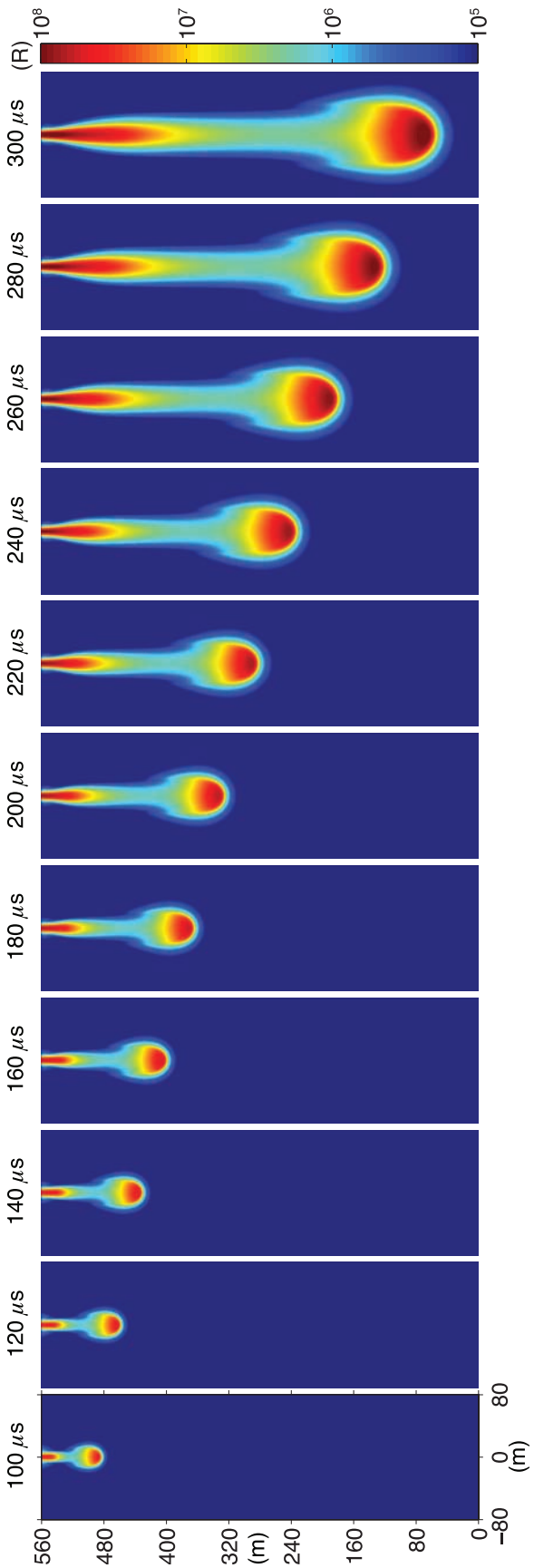

Figure 2. A time sequence of intensity distributions of $1PN_2$ for a downward-propagating model positive streamer at 75-km altitude. The sequence of images is shown with 20-μs interval, starting at 100 μs and ending at 300 μs. The formatting is consistent with that of *Stenbaek-Nielsen et al.* [2007, Figure 2].

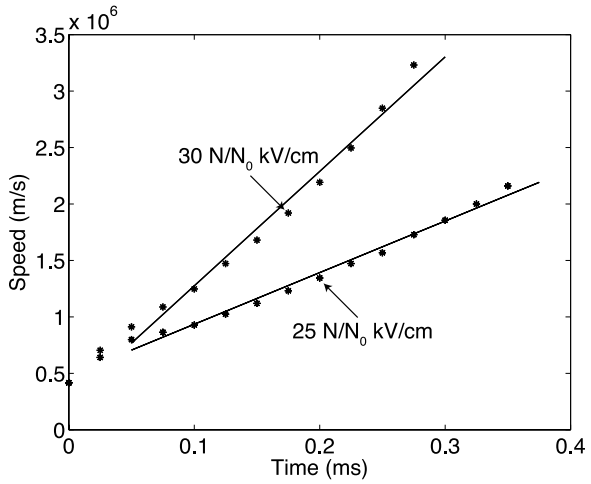

Figure 3. The speed of the model streamer as a function of time for two different applied electric fields: 30 N/N_0 kV/cm and 25 N/N_0 kV/cm. The points represent the speeds computed from the modeling results at individual moments of time, and the solid lines represent the corresponding linear fits.

experimentally observed streamers, and reach characteristics (i.e., speed, brightness) in close agreement with observations at a later instant of time.

[15] The speed of the model streamer for the case of 30 N/N_0 kV/cm reaches a value of 3.2×10^6 m/s at the end of the simulation, which is about 20 times less than the maximum speed $(5-6) \times 10^7$ m/s for observed sprite streamers [e.g., *McHarg et al.*, 2007; *Stenbaek-Nielsen et al.*, 2007]. The discrepancy of a factor of 20 in the speed is not as significant as it seems because the observed maximum speed is for streamers that have traveled much longer distance after initiation than the 550 m of the model streamer. The observed maximum speed can be reached when the model streamer would travel a distance ~10 km (in ~0.8 ms) according to Figure 4. The dependencies documented in Figure 4 also suggest that the observed peak speeds can be reached much faster if the applied electric field exceeds 30 N/N_0 kV/cm.

3.2. Effects of Temporal and Spatial Resolutions

[16] In this section, we present the results demonstrating the effects of different spatial and temporal resolutions on the appearance of streamers.

[17] The intensity distribution of $1PN_2$ (Figure 1c) is shown using the simulation grid with a grid size of 0.4 m × 0.4 m. However, the spatial resolution of the instruments for sprite observations is generally much lower, in order to achieve a reasonable field-of-view for a regular size detector. In Figure 5 we present the same model streamer using four different grid sizes: 5 m × 5 m, 10 m × 10 m, 20 m × 20 m, and 40 m × 40 m. The intensity at each grid point for the reduced resolution image is calculated by averaging the intensities of the original grid points of high-resolution image, which fall in the area covered by that grid point. As the spatial resolution is reduced, the maximum intensity decreases and the streamer becomes more uniform. The lowest resolution of 40 m used for Figure 5 is still higher than the spatial resolution of the observation system used by *McHarg et al.* [2007] and by *Stenbaek-Nielsen et al.* [2007]. For example, the spatial resolution of the detector is 140 m at a distance of 335 km [*Stenbaek-Nielsen et al.*, 2007]. The observations are also affected by atmospheric scattering which in effect will increase the size in the image of what is actually to the detector a point source, e.g., even though stars are true point sources, a bright star will appear in more pixels than a dim star. Hence the larger apparent size of the streamer heads in the observations may only reflect their higher brightness and not necessary a physically larger object (see discussion of this in the work of *Stenbaek-Nielsen et al.* [2007]). However, the effects of the atmospheric scattering are not taken into account in the streamer model. Additionally it should be added that the observations were made using regular camera lenses designed for good focus across the visual range. Most of the sprite emissions are in the near

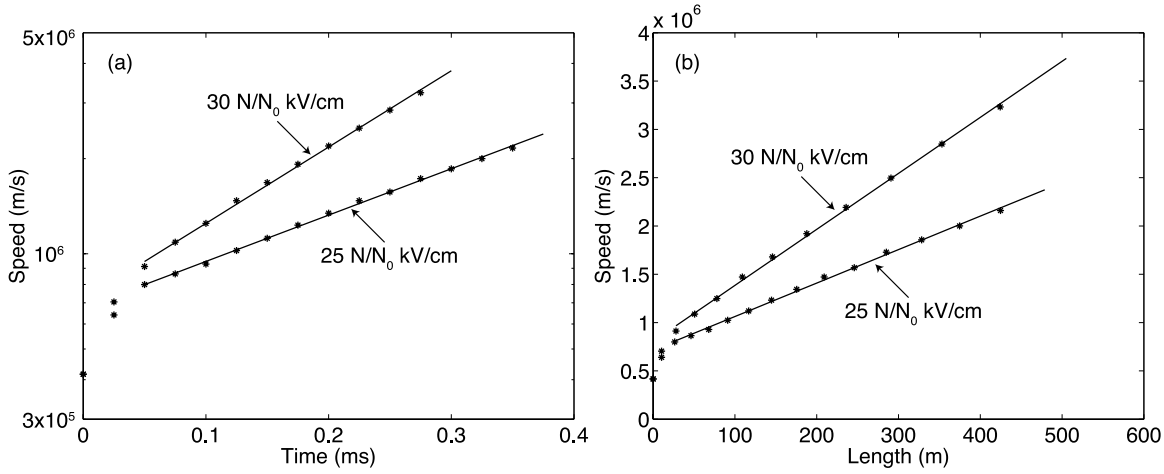

Figure 4. The speed of the model streamer as a function of (a) time and (b) the streamer length for two different applied electric fields: 30 N/N_0 kV/cm and 25 N/N_0 kV/cm. The points represent the speeds computed from the modeling results at the corresponding moments of time, and the solid lines represent the corresponding linear fits. Figure 4a shows the same data set as Figure 3, but here the speed is plotted on a logarithmic scale, which is well approximated by a straight line.

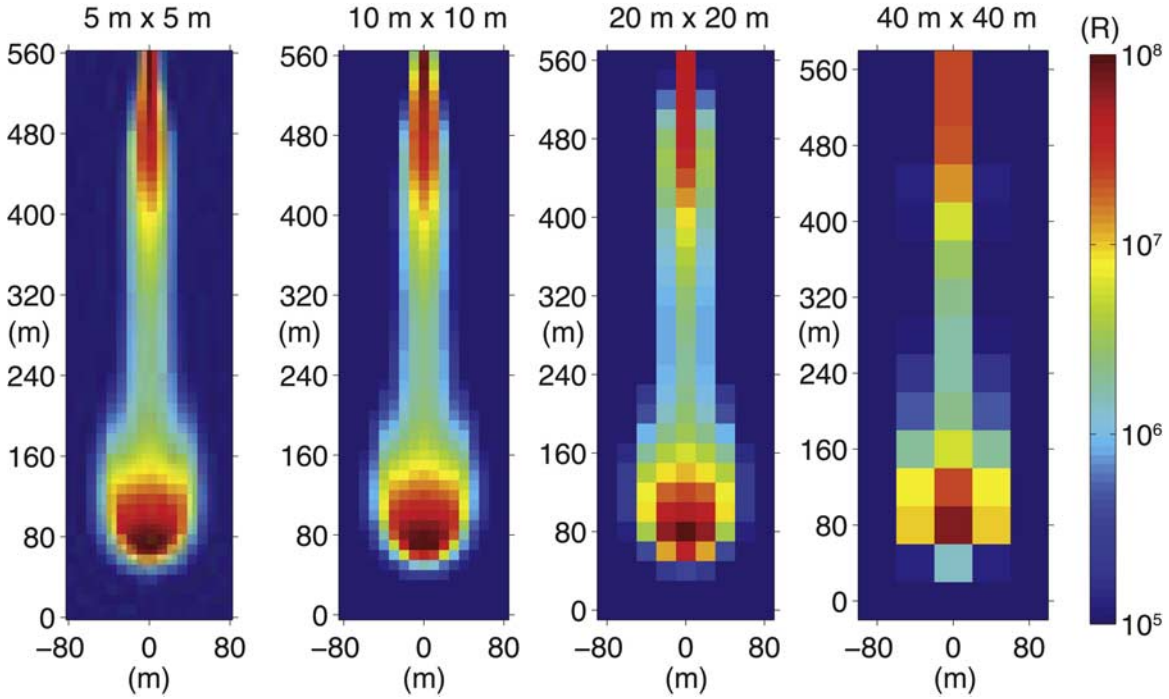

Figure 5. The model streamer represented using different spatial resolutions: 5 × 5 m, 10 × 10 m, 20 × 20 m, and 40 × 40 m. The intensity distributions of $1PN_2$ are plotted here.

infrared which may lead to less than optimum focus of the sprite features. This would also increase their size in the images.

[18] The solution of the streamer model equations requires many time steps with a step size constrained by several conditions for accuracy and stability of the numerical solution [e.g., *Bourdon et al.*, 2007]. For example, it takes more than 12000 time steps to advance the numerical solution to the moment of time 300 μs for the streamer shown in Figure 1. It is impractical to store the results at every time step because of the large amount of data volume involved. In the present study, the modeling results are stored every 0.5 μs. To illustrate the effects of temporal resolution, in Figure 6 we average the emission intensity of $1PN_2$ for a time interval with varying length but fixed ending at 300 μs. Two timescales are important for understanding the time averaging effects: (1) the lifetime of $B^3\Pi_g$ state of N_2 leading to $1PN_2$ emissions is 5.6 μs at 75 km altitude and (2) the time required for the

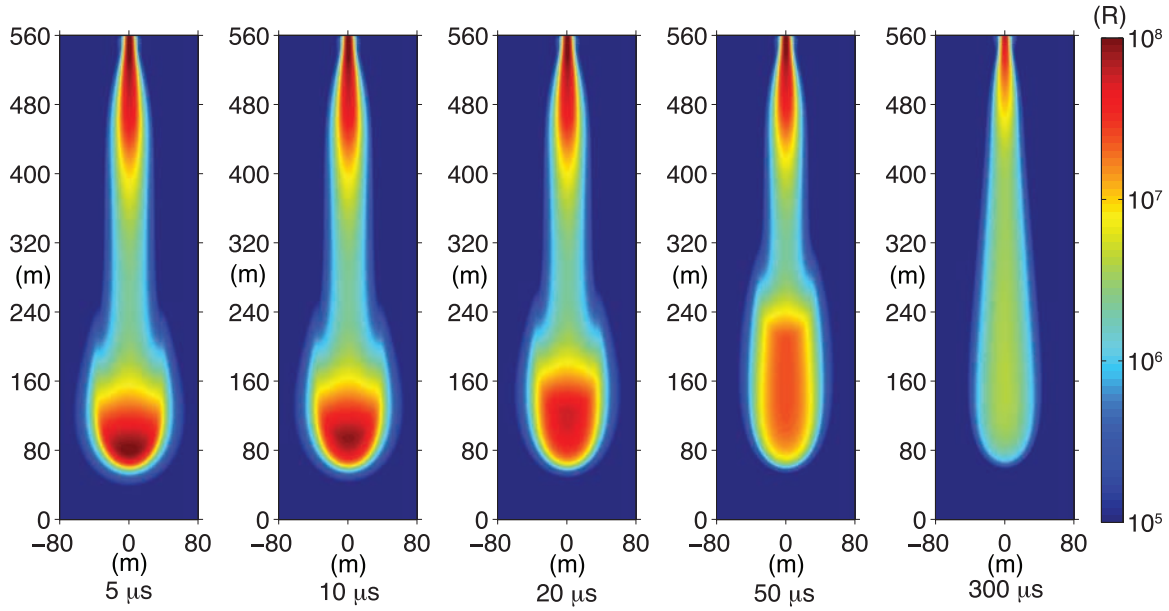

Figure 6. The model streamer represented using different temporal resolutions: 5, 10, 20, 50, and 300 μs. The intensity distributions of $1PN_2$ are plotted here.

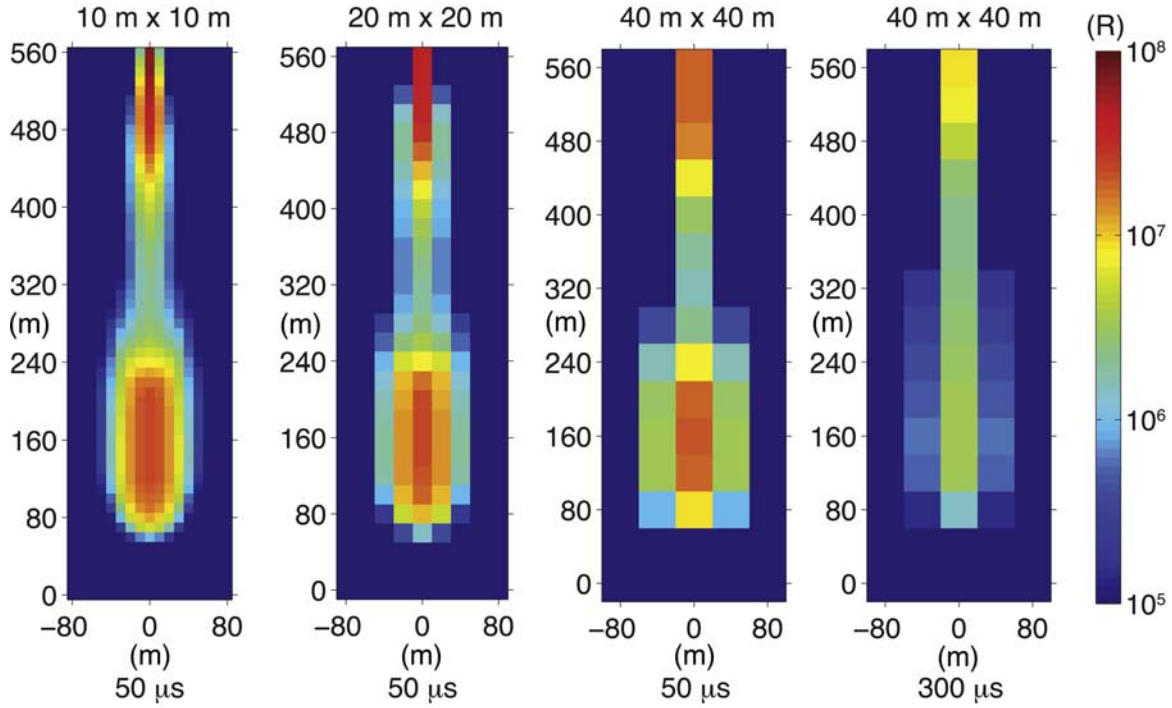

Figure 7. The model streamer represented in different combinations of spatial and temporal resolutions: (50 μs, 10 $\times$ 10 m), (50 μs, 20 $\times$ 20 m), (50 μs, 40 $\times$ 40 m), and (300 μs, 40 $\times$ 40 m). The intensity distributions of $1PN_2$ are plotted here.

streamer to travel the characteristic feature length scale of the streamer. For the streamer presented in Figure 1, the speed at 300 μs is about 3.0×10^6 m/s and the feature length scale is about 10 m. Therefore the corresponding timescale is 3.3 μs. When the time interval for averaging is similar to or less than the shorter one from the two timescales, the result appears very similar to that of the instantaneous model output. The result using an averaging interval of 5 μs appears very similar to the instantaneous intensity distribution at 300 μs (Figure 1c). At a time resolution of 50 μs, the time resolution of the observations by *McHarg et al.* [2007] and *Stenbaek-Nielsen et al.* [2007], the bright streamer head is elongated and the emissions become less structured. A similar elongation is present in the observations consistent with essentially a point source propagating at the observed speed [*Stenbaek-Nielsen et al.*, 2007, Figure 2]. The actual size of the streamer head in the observations is significantly larger than in the simulations, but, as noted above, this may be purely an effect of atmospheric scattering combined with soft focus of near-infrared emissions. Additionally, if we average the streamer emissions over the entire simulation period of 300 μs, a continuous luminous streamer channel forms with a much reduced maximum intensity.

[19] The combined effects of reduced spatial and temporal resolutions are illustrated in Figure 7 considering four sets of spatial and temporal resolutions: (50 μs, 10 $\times$ 10 m), (50 μs, 20 $\times$ 20 m), (50 μs, 40 $\times$ 40 m), and (300 μs, 40 $\times$ 40 m). The brightness of sprites has been estimated as 600 kR from 30 ms video images [*Sentman et al.*, 1995], 12 MR from 1 ms images [*Stenbaek-Nielsen et al.*, 2000], and $\sim$1 GR from 50 μs images [*Stenbaek-Nielsen et al.*, 2007]. The $\sim$1 GR brightness was estimated recognizing that streamer heads are likely smaller than the 140 m spatial resolution in the images; for the $\sim$1GR estimate a 25 m head size was used on the basis of the simulations by *Liu and Pasko* [2004, 2005] that were for shorter streamers at a slightly lower altitude (70 km) than the present study. Figure 7 clearly shows that the reduced maximum emission intensity for the case of low temporal and spatial resolutions is caused by the averaging operation in both space and time. At the temporal resolution of 50 μs, a streamer head distinct from the streamer channel is visible even when the spatial resolution is greatly reduced, consistent with results reported by *McHarg et al.* [2007] and *Stenbaek-Nielsen et al.* [2007]. For the model streamer represented with 50-μs temporal resolution and 40 m $\times$ 40 m spatial resolution, the maximum intensity in the head is about 10 times stronger than that in the channel, which appears to be in general agreement with the observations. However, it must be noted that in the observed images the streamer heads generally saturate the detector which only has 12 bit (4096 counts) dynamic range. Therefore the ratio would likely be somewhat larger than just the image signal ratio. There are also the scattering effects which can greatly affect the recorded differences in the brightness of the head and the channel. For example, while the scatter of the emissions from the streamer head, which to the detector is equivalent to a point source, leads to a larger diameter signal in the image, i.e., expands in 2 dimensions, scatter from the channel only leads to a widening of the channel in the image, i.e., expands in 1 dimension only. In principle it should be possible to model these effects, but we have not attempted this.

3.3. Brightness of Streamers

[20] The brightness of the observed sprite streamer increases as the streamer moves downward [*Stenbaek-Nielsen et al.*, 2007, Figure 2] which results in increasing signal

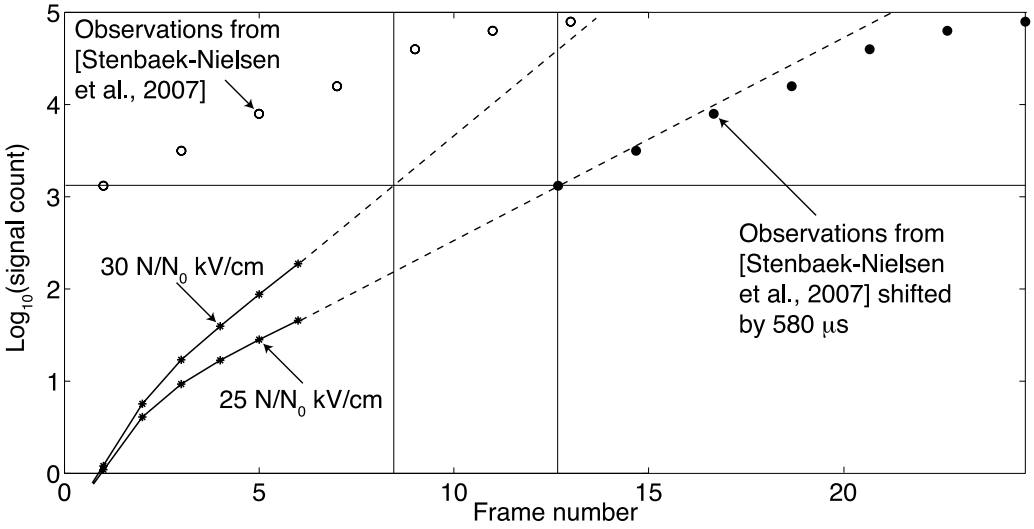

Figure 8. The signal counts as a function of frame number. Circles are the first seven data points presented *Stenbaek-Nielsen et al.* [2007, Figure 3], which correspond to recordings made at 10,000 fps with 50-μs exposure time. The signal counts from the two modeling cases are calculated as if the model streamers are recorded at 20,000 fps with 50-μs exposure time. They are plotted horizontally aligning with the circles at the first frame. The simulations stop at frame 6 when stable streamer characteristics (i.e., acceleration, expansion, etc.) for a given reduced field E/N are already established, and the dashed lines are linear extrapolations of the simulation results. For frames 8–9 and 12–13 for the cases of 30 N/N_0 kV/cm and 25 N/N_0 kV/cm, respectively, the brightness of the model streamers reaches the value corresponding to the first frame of the observed streamer, which suggests that the observed streamer is evolved from the model streamer, and in principle if the simulation runs long enough, the obtained model streamer will show the same characteristics (e.g., speed, brightness) as the observed streamer.

counts as shown in Figure 3 of the same paper. An intensity calibration based on an analysis of star fields recorded for this purpose showed that the photon flux (photons/cm^2/s) in front of the detector is 310 times the signal count in the images recorded at 10,000 fps. This conversion factor was then used to convert the observed streamer head signals into emission rates. We now use the same conversion technique, but in the opposite direction, to convert the model streamer head emissions into image signal counts for a direct comparison of the model with these observations. The distance used from the streamer to the detector is 335 km as given by *Stenbaek-Nielsen et al.* [2007].

[21] The results are shown in Figure 8. The circles in the upper left are the first 7 points from Figure 3 in the work of *Stenbaek-Nielsen et al.* [2007]. The data points are from images recorded at 10,000 fps with 50-μs exposure time, i.e., there is 100 μs between data points. The first point represents the first image with the streamer head clearly identifiable. Thus this data point can be viewed as representing the approximate minimum detection level and is indicated by the horizontal line through the point. The actual streamer initiation is earlier, but the image data cannot provide any information about how much earlier. The model data points are shown in the lower left of the Figure 8. The model points are derived from the model data reported earlier in this paper, i.e., 20,000 fps with 50-μs exposure time and for 2 values of the sprite-driving electric field, 25 N/N_0 kV/cm and 30 N/N_0 kV/cm. For both field values the signal count is seen to increase rapidly initially but then levels off to an electric field-dependent constant slope in the logarithmic scale plot. The slope is larger for the larger electric field. The slope of the observations is very close to that of the 25 N/N_0 kV/cm case indicating that the observed streamer was developing in a lightning induced electric field of this magnitude. This result is consistent with a conclusion obtained in a recent comparison study of sprite video observations and numerical simulations of electromagnetic fields produced by cloud-to-ground lightning discharges by *Hu et al.* [2007] which shows that bright, short-delayed sprites are initiated when the lightning field reaches magnitudes exceeding 80% of the conventional breakdown threshold field.

[22] As mentioned above the optical observations have no information about the time of streamer initiation, but extrapolating the model data would suggest that the first observational data point should be near 580 μs after streamer initiation. With the observed data points shifted 580 μs, as shown in the upper right of Figure 8, they agree well with the extrapolated model brightness for a field of 25 N/N_0 kV/cm. At this time, extrapolating the model speeds shown in Figure 4a, the model predicts a speed of the streamer of $\sim 5 \times 10^6$ m/s which is also in good agreement with the observations (speed derived from the work of *Stenbaek-Nielsen et al.* [2007, Figure 2]).

[23] The previous studies [e.g., *Liu and Pasko*, 2004] have established that for streamers propagating in strong fields their radius r_s and speed $v_s = dL/dt$ increase linearly proportionally to the streamer length L (see, for example, Figure 4b). Since in this case $dv_s/dL = \text{const}$, and $dv_s/dL = dv_s/dt/(dL/dt) = d \ln v_s/dt$, the velocity of the accelerating streamer is exponentially increasing in time, as illustrated in Figure 4a. This analysis indicates that the acceleration of the streamer also exponentially increases in time and related e-folding time

constant, the same for both velocity and acceleration, can be determined as inverse of slopes determined in Figure 4 and discussed in section 3.1 (i.e., $1/5.8 \times 10^3$ s^{-1} = 0.172 ms, and $1/3.5 \times 10^3$ s^{-1} = 0.286 ms, for the fields 30 N/N_0 kV/cm and 25 N/N_0 kV/cm, respectively). Because of the linear relationship between v_s and r_s and the fact that the brightness of the streamer increases proportionally to the streamer radius ($\sim r_s$), a similar exponential relationship can be established for total number of photons emitted by streamer and counts per unit time ($\sim r_s^3$), which justifies the linear extrapolation in Figure 8. Indeed, the slope of the straight line for the 25 N/N_0 kV/cm case in Figure 8 is 4.77×10^3 1/s (1 frame = 50 μs), which takes a value of $4.77 \times 10^3 \times \ln(10) = 1.098 \times 10^4$ 1/s if we consider the corresponding exponential growth rate. This value is very close to 3 times the exponential growth rate of radius $3 \times 3.5 \times 10^3 = 1.05 \times 10^4$ 1/s, as it should be because of the $\sim r_s^3$ dependence of signal counts on the streamer radius. This argument leads to a simple approach to obtain the exponential growth rate of the radius and velocity of sprite streamers by measuring the growth rate of the total number of photons emitted by the streamer per second. The direct measurement of the growth rate of the radius and velocity may be difficult because of atmospheric scattering effects as discussed in section 3.2. We emphasize again that the discussed relationship remains exact only under assumption that the E/N remains constant along the entire streamer trajectory. Because of the general altitude distribution of the electric field driving sprites [e.g., *Pasko et al.*, 2000] it is likely that long sprite streamers move to a region of reduced E/N values as they propagate to lower altitudes. This may result in a significant reduction in the growth rate of the signal counts at later moments of time observed by *Stenbaek-Nielsen et al.* [2007, Figure 3] and partially reproduced in Figure 8 of the present paper.

[24] The analysis presented above suggests a simple method for the remote sensing of the sprite-driving field in the upper mesosphere and the lower ionosphere. As illustrated in Figure 8 the rate of change in the brightness of the streamer head appears to be closely related to the driving electric field. The change in brightness and the streamer velocities are parameters that are relatively easy to extract from high-speed images, and hence the high-speed observations together with the modeling can yield the sprite-driving electric field.

4. Summary and Conclusions

[25] The modeling results for positive streamers propagating in two different fields: 30 N/N_0 and 25 N/N_0 kV/cm indicate that streamers propagate with acceleration and expansion, consistent with previous modeling results [*Babaeva and Naidis*, 1997; *Kulikovsky*, 1997; *Liu and Pasko*, 2004]. The acceleration calculated from modeling results is in a good agreement with the values derived from the high-speed video observations of sprite streamers [*McHarg et al.*, 2007; *Stenbaek-Nielsen et al.*, 2007].

[26] To further compare the modeling results with the high-speed video data, we explore the effects of different spatial and temporal resolutions of an observation system on the visual appearances of sprite streamers. It is found that the large variation in brightness of sprites estimated from several observational studies is due to different temporal and spatial resolutions of the instrument in use. The streamer appears dimmer and less structured in images with low spatial and temporal resolutions.

[27] Mainly due to the increasing radius of the streamer head, the brightness of the streamer head increases as the streamer continues to propagate. The comparison results demonstrate that the brightness of a sprite streamer head increases exponentially in time and can span more than 4 orders of magnitude in a very short period of about 1.25 ms. The rate of increase depends on the magnitude of the applied electric field. This functional dependence can be used for remote sensing of the ambient electric field driving sprites at the mesospheric and lower ionospheric altitudes by measuring changes in brightness. The comparison between the modeling results and the observational data in terms of the changing rate of the brightness of the sprite streamer demonstrates that the sprite event observed by *McHarg et al.* [2007] and *Stenbaek-Nielsen et al.* [2007] was initiated with streamers propagating in strong electric fields close to the conventional breakdown threshold.

[28] **Acknowledgments.** This research was supported by the Physics and Space Sciences Department of Florida Institute of Technology and by NSF grants ATM 0725360 and ATM 0734083 to Penn State University, NSF grant ATM 0737605 to University of Alaska Fairbanks, and NSF grant ATM 0334521 to US Air Force Academy.

[29] Zuyin Pu thanks the reviewers for their assistance in evaluating this paper.

References

Babaeva, N. Y., and G. V. Naidis (1997), Dynamics of positive and negative streamers in air in weak uniform electric fields, *IEEE Trans. Plasma Sci.*, *25*, 375–379.

Barrington-Leigh, C. P., U. S. Inan, M. Stanley, and S. A. Cummer (1999), Sprites triggered by negative lightning discharges, *Geophys. Res. Lett.*, *26*, 3605–3608.

Barrington-Leigh, C. P., U. S. Inan, and M. Stanley (2001), Identification of sprites and elves with intensified video and broadband array photometry, *J. Geophys. Res.*, *106*, 1741–1750.

Bourdon, A., V. P. Pasko, N. Y. Liu, S. Célestin, P. Ségur, and E. Marode (2007), Efficient models for photoionization produced by non-thermal gas discharges in air based on radiative transfer and the Helmholtz equations, *Plasma Sources Sci. Technol.*, *16*, 656–678, doi:10.1088/0963-0252/16/3/026.

Briels, T. M. P., J. Kos, E. M. van Veldhuizen, and U. Ebert (2006), Circuit dependence of the diameter of pulsed positive streamers in air, *J. Phys. D Appl. Phys.*, *39*, 5201–5210.

Cummer, S. A., N. C. Jaugey, J. B. Li, W. A. Lyons, T. E. Nelson, and E. A. Gerken (2006), Submillisecond imaging of sprite development and structure, *Geophys. Res. Lett.*, *33*, L04104, doi:10.1029/2005GL024969.

Ebert, U., C. Montijn, T. M. P. Briels, W. Hundsdorfer, B. Meulenbroek, A. Rocco, and E. M. van Veldhuizen (2006), The multiscale nature of streamers, *Plasma Sources Sci. Technol.*, *15*, S118–S129.

Gerken, E. A., and U. S. Inan (2002), A survey of streamer and diffuse glow dynamics observed in sprites using telescopic imagery, *J. Geophys. Res.*, *107*(A11), 1344, doi:10.1029/2002JA009248.

Gerken, E. A., and U. S. Inan (2003), Observations of decameter-scale morphologies in sprites, *J. Atmos. Sol. Terr. Phys.*, *65*, 567–572, doi:10.1016/S1364-6826(02)00333-4.

Gerken, E. A., U. S. Inan, and C. P. Barrington-Leigh (2000), Telescopic imaging of sprites, *Geophys. Res. Lett.*, *27*, 2637–2640.

Hampton, D. L., M. J. Heavner, E. M. Wescott, and D. D. Sentman (1996), Optical spectral characteristics of sprites, *Geophys. Res. Lett.*, *23*, 89–93.

Hu, W. Y., S. A. Cummer, and W. A. Lyons (2007), Testing sprite initiation theory using lightning measurements and modeled electromagnetic fields, *J. Geophys. Res.*, *112*, D13115, doi:10.1029/2006JD007939.

Kanmae, T., H. C. Stenbaek-Nielsen, and M. G. McHarg (2007), Altitude resolved sprite spectra with 3 ms temporal resolution, *Geophys. Res. Lett.*, *34*, L07810, doi:10.1029/2006GL028608.

Kulikovsky, A. A. (1997), The mechanism of positive streamer acceleration and expansion in air in a strong external field, *J. Phys. D Appl. Phys.*, *30*, 1515–1522.

Liu, N. Y., and V. P. Pasko (2004), Effects of photoionization on propagation and branching of positive and negative streamers in sprites, *J. Geophys. Res.*, *109*, A04301, doi:10.1029/2003JA010064.

Liu, N. Y., and V. P. Pasko (2005), Molecular nitrogen LBH band system far-UV emissions of sprite streamers, *Geophys. Res. Lett.*, *32*, L05104, doi:10.1029/2004GL022001.

Liu, N. Y., and V. P. Pasko (2006), Effects of photoionization on similarity properties of streamers at various pressures in air, *J. Phys. D Appl. Phys.*, *39*, 327–334, doi:10.1088/0022-3727/39/2/013.

Liu, N. Y., S. Célestin, A. Bourdon, V. P. Pasko, P. Ségur, and E. Marode (2008), Photoionization and optical emission effects of positive streamers in air at ground pressure, *IEEE Trans. Plasma Sci.*, *36*(4), 942–943.

Loeb, L. B., and J. M. Meek (1940), The mechanism of spark discharge in air at atmospheric pressure, *J. Appl. Phys.*, *11*, 438–447.

Marshall, R. A., and U. S. Inan (2005), High-speed telescopic imaging of sprites, *Geophys. Res. Lett.*, *32*, L05804, doi:10.1029/2004GL021988.

Marshall, R. A., and U. S. Inan (2006), High-speed measurements of small-scale features in sprites: Sizes and lifetimes, *Radio Sci.*, *41*, RS6S43, doi:10.1029/2005RS003353.

McHarg, M. G., R. K. Haaland, D. R. Moudry, and H. C. Stenbaek-Nielsen (2002), Altitude-time development of sprites, *J. Geophys. Res.*, *107*(A11), 1364, doi:10.1029/2001JA000283.

McHarg, M. G., H. C. Stenbaek-Nielsen, and T. Kammae (2007), Streamer development in sprites, *Geophys. Res. Lett.*, *34*, L06804, doi:10.1029/2006GL027854.

Mende, S. B., R. L. Rairden, G. R. Swenson, and W. A. Lyons (1995), Sprite spectra: N_2 1 PG band identification, *Geophys. Res. Lett.*, *22*, 2633–2637.

Moudry, D. R., H. C. Stenbaek-Nielsen, D. D. Sentman, and E. M. Wescott (2002), Velocities of sprite tendrils, *Geophys. Res. Lett.*, *29*(20), 1992, doi:10.1029/2002GL015682.

Moudry, D. R., H. C. Stenbaek-Nielsen, D. D. Sentman, and E. M. Wescott (2003), Imaging of elves, halos and sprite initiation at 1 ms time resolution, *J. Atmos. Sol. Terr. Phys.*, *65*, 509–518, doi:10.1016/S1364-6826(02)00323-1.

Pasko, V. P. (2007), Red Sprite discharges in the atmosphere at high altitude: The molecular physics and the similarity with laboratory discharges, *Plasma Sources Sci. Technol.*, *16*, 13–29, doi:10.1088/0963-0252/16/1/S02.

Pasko, V. P., U. S. Inan, and T. F. Bell (1998), Spatial structure of sprites, *Geophys. Res. Lett.*, *25*, 2123–2126.

Pasko, V. P., U. S. Inan, and T. F. Bell (2000), Fractal structure of sprites, *Geophys. Res. Lett.*, *27*, 497–500.

Raizer, Y. P. (1991), *Gas Discharge Physics*, Springer, New York.

Sentman, D. D., E. M. Wescott, D. L. Osborne, D. L. Hampton, and M. J. Heavner (1995), Preliminary results from the Sprites94 campaign: Red sprites, *Geophys. Res. Lett.*, *22*, 1205–1208.

Sentman, D. D., H. C. Stenbaek-Nielsen, M. G. McHarg, and J. S. Morrill (2008), Plasma chemistry of sprite streamers, *J. Geophys. Res.*, *113*, D11112, doi:10.1029/2007JD008941.

Shcherbakov, Y. V., and R. S. Sigmond (2007), Subnanosecond spectral diagnostics of streamer discharges. I: Basic experimental results, *J. Phys. D Appl. Phys.*, *40*, 460–473, doi:10.1088/0022-3727/40/2/023.

Stanley, M., P. Krehbiel, M. Brook, C. Moore, W. Rison, and B. Abrahams (1999), High speed video of initial sprite development, *Geophys. Res. Lett.*, *26*, 3201–3204.

Stenbaek-Nielsen, H. C., D. R. Moudry, E. M. Wescott, D. D. Sentman, and F. T. São Sabbas (2000), Sprites and possible mesospheric effects, *Geophys. Res. Lett.*, *27*, 3829–3832.

Stenbaek-Nielsen, H. C., M. G. McHarg, T. Kammae, and D. D. Sentman (2007), Observed emission rates in sprite streamer heads, *Geophys. Res. Lett.*, *34*, L11105, doi:10.1029/2007GL029881.

Taylor, M. J., et al. (2008), Rare measurements of a sprite with halo event driven by a negative lightning discharge over Argentina, *Geophys. Res. Lett.*, *35*, L14812, doi:10.1029/2008GL033984.

van Veldhuizen, E. M., and W. R. Rutgers (2002), Pulsed positive corona streamer propagation and branching, *J. Phys. D Appl. Phys.*, *35*, 2169–2179.

van Veldhuizen, E. M., P. C. M. Kemps, and W. R. Rutgers (2002), Streamer branching in a short gap: The influence of the power supply, *IEEE Trans. Plasma Sci.*, *30*, 162–163.

K. Adams and V. P. Pasko, Communications and Space Sciences Laboratory, Department of Electrical Engineering, Pennsylvania State University, University Park, PA 16802, USA. (kla193@psu.edu; vpasko@psu.edu)

N. Y. Liu, Geospace Physics Laboratory, Department of Physics and Space Sciences, Florida Institute of Technology, 348 Olin Physics Science Building, Melbourne, FL 32901, USA. (nliu@fit.edu)

M. G. McHarg, Department of Physics, United States Air Force Academy, CO 80840, USA. (matthew.mcharg@usafa.edu)

H. C. Stenbaek-Nielsen, Geophysical Institute, University of Alaska, Fairbanks, AK 99775, USA. (hnielsen@gi.alaska.edu)